



AN EQUATION OF STATE FOR LAND SURFACE CLIMATES

KLAUS FRAEDRICH* and FRANK SIELMANN†

*Meteorologisches Institut,
Universität Hamburg, Hamburg, Germany*

**klaus.fraedrich@zmaw.de*

†frank.sielmann@zmaw.de

Received October 1, 2010; Revised January 15, 2011

A biased coinflip Ansatz provides a stochastic regional scale surface climate model of minimum complexity, which represents physical and stochastic properties of the rainfall–runoff chain. The solution yields the Schreiber–Budyko relation as an equation of state describing land surface vegetation, river runoff and lake areas in terms of physical flux ratios, which are associated with three thresholds. Validation of consistency and predictability within a Global Climate Model (GCM) environment demonstrates the stochastic rainfall–runoff chain to be a viable surrogate model for regional climate state averages and variabilities. A terminal (closed) lake area ratio is introduced as a new climate state parameter, which quantifies lake overflow as a threshold in separating water from energy limited climate regimes. A climate change analysis based on the IPCC A1B scenario is included for completeness.

Keywords: Equation of climate states; land surface climate; vegetation; rivers; lakes; stochastic climate models; biased coinflip.

1. Introduction

The surface cover of the Earth links soil and atmosphere, and determines climate and life [Vernadsky, 1926/1998]. Thus it is not surprising that climate analysis favors two approaches tending either more to the physical or to the life sciences: Physical climate analysis is based on the underlying dynamical concepts, which are represented by mass, momentum, energy or entropy balance equations derived from the related state variables or observables. A more life sciences or phenomenological approach is based on parameterizations that describe, for example, plants and biomes and, therefore perhaps more suitably, stochastic concepts, which provide functional relationships.

First quantitative steps on the more phenomenology oriented track were made by Köppen [1936], who introduced a climate classification that

relates physical climate variables to vegetation types. Later, Budyko [1974] summarized research on biome related climatology in his seminal book on *Climate and Life*. He interpreted empirical relations (see e.g. [Schreiber, 1904]) by combining dimensionless numbers, based on energy and water flux ratios, with geo-botanic phenomena. Applications to global climate change observations and climate models commenced in the 1990s employing Köppen’s biome types (see, for example, [Guetter & Kutzbach, 1990]) or Budyko’s indices [Koster & Suarez, 1999; Arora, 2002]. And, more recently, theoretical underpinning has been provided, which is based on a stochastic interpretation of the empirical relation entering Budyko’s climate analysis of the Earth’s vegetation [Fraedrich, 2010].

Here we introduce a diagnostics of climate and life on the Earth’s land surface, which is based on

thresholds and a novel stochastic-dynamic interpretation of an empirical relation between the longterm surface energy and water exchange. This includes the identification of surface climate states and supplements the traditional climate analysis based on the common dynamical circulation statistics. Section 2 describes a stochastic-dynamic model underlying the rainfall–runoff chain and derives functional relations for mean climate indicators. Validation in a Global Climate Model (GCM) environment is provided for the subsequent spectrum of applications. Section 3 analyzes the climate means projected on the distribution of vegetation. Section 4 describes the climate variability focusing on river runoff. Section 5 introduces lakes and their areas as a novel climate indicator, which relates the energy and water flux balances of the land surface; it also includes present and future climate state analyses. In the outlook (Sec. 6) potential future applications are discussed.

2. An Equation of State for Ideal Climates

Land surface climates on catchment scale are controlled by long time means (capital letters) of precipitation P , representing the atmospheric water supply, and net radiation N , as the atmospheric water demand, both of which balance the water and energy flux at land surfaces (defined by the water equivalents of energy units)

$$P = Ro + E \quad (1)$$

$$N = E + H. \quad (2)$$

Flux partitioning into runoff Ro plus evaporation E at the ground, and into sensible heat H plus moisture fluxes E , to the atmosphere, is due to processes comprising the rainfall–runoff chain linking atmosphere, biosphere and pedosphere. A biased coinflip model of the rainfall–runoff chain is introduced to provide a stochastic catchment scale climate model; it connects the fast biosphere with the slow soil water reservoir to obtain the surface climate in terms of a functional relation similar to an equation of state. The subsequent short introduction follows Fraedrich [2010]. (i) Given the atmospheric water input, the rainfall–runoff chain over continents commences with the fast stochastic water reservoir of the biosphere. Its small capacity (that is, interception in vegetation and wetted ground) is limited by a vegetation type dependent threshold determined by the total available energy supply. (ii) The

water surplus from the fast reservoir feeds the slow (almost stationary) soil moisture reservoir of large capacity and long time scale thus balancing (and averaging) the runoff at the end after taking the climate average. The resulting mean water flux partitioning between runoff and evaporation depends on the water demand–supply ratio, which is characterized by a threshold separating water from energy limited climate regimes.

2.1. Rainfall–runoff chain: A stochastic-dynamic Ansatz

To a good approximation daily rainfall p_k is exponentially distributed which, as a maximum entropy distribution, holds within the $[0, \infty)$ -domain with the mean rainfall total P [Eagleson, 1978; Rodriguez-Iturbe *et al.*, 1999]

$$\text{prob}(p_k \leq p^*) = 1 - \exp\left(\frac{-p^*}{P}\right). \quad (3)$$

Rainfall occurring randomly suggests a biased coinflip model for a simulator of daily rainfall exceeding ($p^* \geq N$) or staying below ($p^* < N$) a given threshold N . This affects the following two water reservoirs, which respond to the water input: first, the shallow and fast biosphere and, subsequently, the deep and slow soil, whose water holding capacities and residence times differ by orders of magnitude.

2.1.1. Fast reservoir (microstate)

The biosphere represents the fast reservoir, which is characterized by a net radiation threshold and a short water residence time. Its water holding capacity, which comprises interception in vegetation and wetted ground, captures the rainfall before it enters subsurface processes with runoff [Savenije, 2004]; that is, rainfall and interception are merely water in transit. Furthermore, the biosphere’s vegetation spectrum ranges from tropical forests, which are characterized by large net radiation N , to tundra with small N (see [Budyko, 1974, Figure 104]). This has the following consequences: First, the intercepted water amount is subject to the almost constant net radiation $n_k \sim N$ [Sharif *et al.*, 2007, Appendix; Arora, 2002], whose water equivalent (per day) represents the water demand of the daily water supply. That is, rainfall exceeding the net radiation enters the soil and runoff processes while the rest evaporates. Secondly, net radiation provides a natural upper limit of the water demand; thus it

also represents the biosphere’s water holding capacity, which differs for the various types of vegetation and their fast (order of days) response to daily rainfall supply. In this sense, net radiation provides a natural biospheric (first) threshold, which is related to the short term daily rainfall processes affecting interception

$$p_k \leq N \quad \text{or} \quad p_k > N \tag{4}$$

That is, within the biosphere, the rainfall–runoff chain attains two states, which are associated with two mutually exclusive occurrence probabilities: q_0 or $q_1 = 1 - q_0$.

- (1) On a q_0 -day, the biosphere’s capacity exceeds the rainfall supply p_k with probability

$$\begin{aligned} q_0 &= \text{prob}(p_k \leq N) = \int_0^N f(p_k) dp_k \\ &= 1 - \exp\left(\frac{-N}{P}\right). \end{aligned} \tag{5}$$

On that day, the larger water demand N provides sufficient energy to completely evaporate the rainfall, $e_k = p_k$, while the remaining part of the net radiation is available for sensible heat flux, $h_k = N - e_k$, to the atmosphere; thus the reservoir can start anew as empty on the following day.

- (2) A q_1 -day’s rainfall supply p_k exceeding the capacity occurs with probability

$$\begin{aligned} q_1 &= \text{prob}(p_k > N) = \int_N^\infty f(p_k) dp_k \\ &= \exp\left(\frac{-N}{P}\right). \end{aligned} \tag{6}$$

Part of the rainfall is intercepted and evaporates completely up to $e_k = n_k = N$, while the remaining surplus, $p_k - e_k = r_{o_k}$, enters the deep and slow soil water reservoir and the shallow reservoir also commences anew. This yields a biased coin-flip process characterizing the microscopic statistics of the rainfall–runoff chain of the fast and shallow reservoir.

2.1.2. Slow reservoir (macrostate)

The slow or soil water reservoir is characterized by a very long water residence time. Its fluxes represent the last or discharge processes in the rainfall–runoff chain which, after integrating the fast reservoir’s water surplus, provide the river runoff, Ro . It acts

with an almost infinite residence time, because its moisture capacity is much larger than any fluxes of water during the short time interval of a day, and it is considered stationary compared to the effect of these fluxes. The random water surplus r_{o_k} by the fast reservoir balances, in the climate mean, the slow soil water reservoir’s discharge Ro . Integration over the coinflip’s q_1 -state occurrences suffices to obtain the climate mean runoff; that is, the mean daily rainfall, which exceeds the fast reservoir’s capacity, $\int_N^\infty p_k \exp(-p_k/P) dp_k/P$, is reduced by the total maximum possible daily evaporation, $\int_N^\infty N \exp(-p_k/P) dp_k/P$, before entering the slow reservoir as surplus. The mean provides the accumulated runoff. When transformed to the evaporation ratio, the Schreiber [1904] formula is reproduced

$$F^* = \frac{E}{P} = 1 - \exp\left(\frac{-N}{P}\right) \tag{7}$$

which partitions the atmospheric water supply (or rainfall) P , into river runoff, Ro , and evaporation, E , from water catchments, $Ro = P - E$.

2.2. Climate state diagram

Further mean flux ratios can be introduced to characterize the climate states of the biased coinflip rainfall–runoff chain. Besides the evaporation ratio (7) or Schreiber [1904] formula this is the runoff ratio

$$C = \frac{Ro}{P} = 1 - F \tag{8}$$

which, for the biased coinflip Ansatz, is formulated as $C^*(D) = 1 - F^*$ (analyzed in Sec. 4). Another ratio depends on the water demand (or net radiation) N , over the water supply P . This ratio is the dryness ratio [Budyko, 1974] and emerges in the rainfall–runoff chain as a constant for the ideal climate of the Earth’s surface, $D = N/P > 0$. It provides a globally relevant second threshold which, at $D = 1$, separates water limited climates, $N > P$, from energy limited regimes, $P \geq N$, when water demand exceeds supply:

$$D = \frac{N}{P} : D \leq 1 \quad (P \geq N) \quad \text{or} \quad D > 1 \quad (N > P). \tag{9}$$

Furthermore, the dryness ratio D is also a quantitative indicator for the climate-vegetation relation [Budyko, 1974]: Tundra, $D < 1/3$, and forests, $1/3 < D < 1$, are energy limited because available

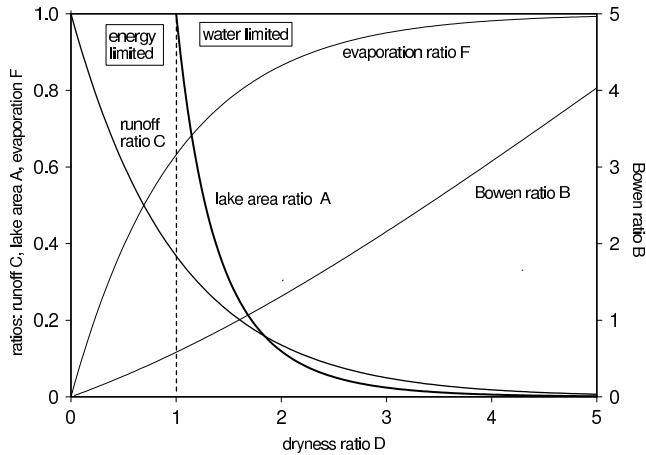


Fig. 1. Ratios of mean fluxes of the stochastic rainfall-runoff chain: Bowen ratio B , runoff ratio C , and evaporation ratio F depending on the climate indicator (or constant) D . The lake area ratio A is introduced in Sec. 4.

energy N is low, so that runoff exceeds evaporation for given precipitation, $E \sim N$. Steppe and Savanna, $1 < D < 2.0$, semi-desert $2.0 < D < 3.0$, and desert $3.0 < D$, are water limited climates, where the available energy is so high that water supplied by precipitation evaporates, which then exceeds runoff, $E \sim P$. Finally, the Bowen ratio, $B = E/H$ can also be deduced; after employing the water and energy flux balance equations (1 and 2) one obtains $B^* = D/F - 1$.

Summarizing: The Earth surface climate states are characterized by mean flux ratios (Fig. 1). They are part of the equation of state and the rainfall-runoff chain, which is generated by microstate fluctuations of rainfall, modulated by the biospheric interception, and averaged in the slow soil reservoir. In the following we validate the rainfall-runoff state equation within a coupled Global Climate Model (GCM) environment, because it provides physically consistent data sets.

3. Climate Means and Vegetation: Evaporation Ratio

The climates associated with the stochastic land surface model of rainfall-runoff chain (7) are analyzed using simulations of a coupled atmosphere-ocean global climate model (GCM). The model simulations are based on a state of the art coupled atmosphere-ocean GCM providing long term nine-neighbor means of continental grid points simulated by a 20th century control run (1958–2001, IPCC-AR4 MPI-ECHAM5-T63L31 coupled to MPI-OM-GR1.5L40 GR1, run on a NEC-SX with resolution

T63 (1.875°), N48) using observed anthropogenic forcings by CO_2 , CH_4 , N_2O , CFCs, O_3 and sulfate [Roeckner *et al.*, 2006; Hagemann *et al.*, 2006]. The annual mean data sets form the basis of the subsequent analyses.

3.1. Budyko's dryness ratio and Koeppen's climate classes

The global distribution of Budyko's dryness ratio D , which is the fundamental climate state parameter of the rainfall-runoff chain, is shown in Fig. 2(a). For comparison, the commonly used Koeppen classification [Köppen, 1936] is also presented [Fig. 2(b)] with its main types of tropical, dry, subtropical, temperate, boreal (cold) and ice climates (see, for example, [Fraedrich *et al.*, 2001, Table 1]), which are commonly attached with the letters A to F, respectively. Note that the dryness ratio D is a continuously varying parameter while the Koeppen classes are discrete. The main difference between both classifications occurs in the tropical and temperate climates related to forest vegetation. These are clearly distinct climate types in the Koeppen scheme while, for Budyko's dryness ratio, forests (ranging from tropical rain to temperate needle leaf vegetation) occur within a relatively small D -interval. The following validation is based on the global maps shown in Fig. 2.

3.2. Validation

The stochastic rainfall-runoff chain is validated in two steps. First, consistency is analyzed comparing the biased coinflip climate states with those of the coupled GCM by binning flux ratios directly and in terms of Koeppen climate types. Then the stochastic model prediction (7) of the mean dryness ratio, based on the input of the coupled GCM evaporation ratio, $F^* = E/P = 1 - \exp(-D)$, is compared with the GCM dryness ratio, $D = N/P$ as the verification:

- (1) *Consistency:* Consistency is analyzed in (D, F) -diagrams [Fig. 3(a)] comparing the biased coinflip state equation with the coupled GCM simulation. First, the (D, F) -ratios of the rainfall-runoff chain are sampled in bins of the dryness ratio D dependent evaporation ratio F , which yields averages and standard deviations [horizontal lines centred on the bin-average, Fig. 3(a)]. These binned averages follow closely

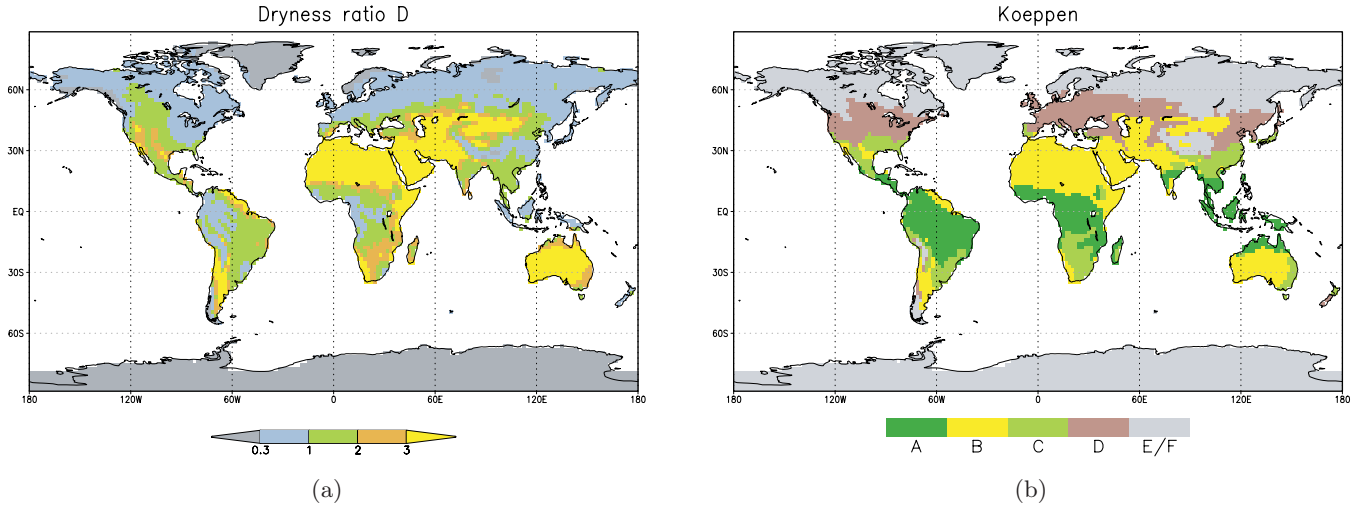


Fig. 2. Present day surface climates based on a state of the art coupled atmosphere-ocean GCM (ECHAM5 20C): (a) Dryness index D for Tundra $D < 1/3$, and forests $1/3 < D < 1$, Steppe and Savanna $1 < D < 2$, semi-desert $2 < D < 3$, desert $3 < D$. (b) Koeppen climate types are tropical (A), dry (B), subtropical (C), temperate (D), boreal and ice (E, F).

the biased coinflip equation of state (7) and, as expected, the variability (standard deviations) increases considerably with increasing dryness. Secondly, besides the flux dependent binning, consistency is also tested by sampling the (D, F) -ratios for the main Koeppen classes (A to F). The sample averages and standard deviations (vertical and horizontal axes centred on the means) show the following results [Fig. 3(b)]: (i) The discrete Koeppen climate type dependent (D, F) -sample means are well aligned along the continuous (dashed) rainfall-runoff chain's evaporation ratio F^* (7).

(ii) The standard deviations of these Koeppen samples embed the theoretical rainfall-runoff chain. Not unexpected, the spread of the dry climate B covers a wide D -range. (iii) The D -locations and the sample means of main Koeppen classes may not necessarily represent the same biospheric properties. This, however, may be achieved by suitably regrouping the Koeppen climate types (including their subclasses; see, for example, [Hanasaki *et al.*, 2008]), which considerably improves the dryness ratio or D -locations associated with the Koeppen climates (not shown).

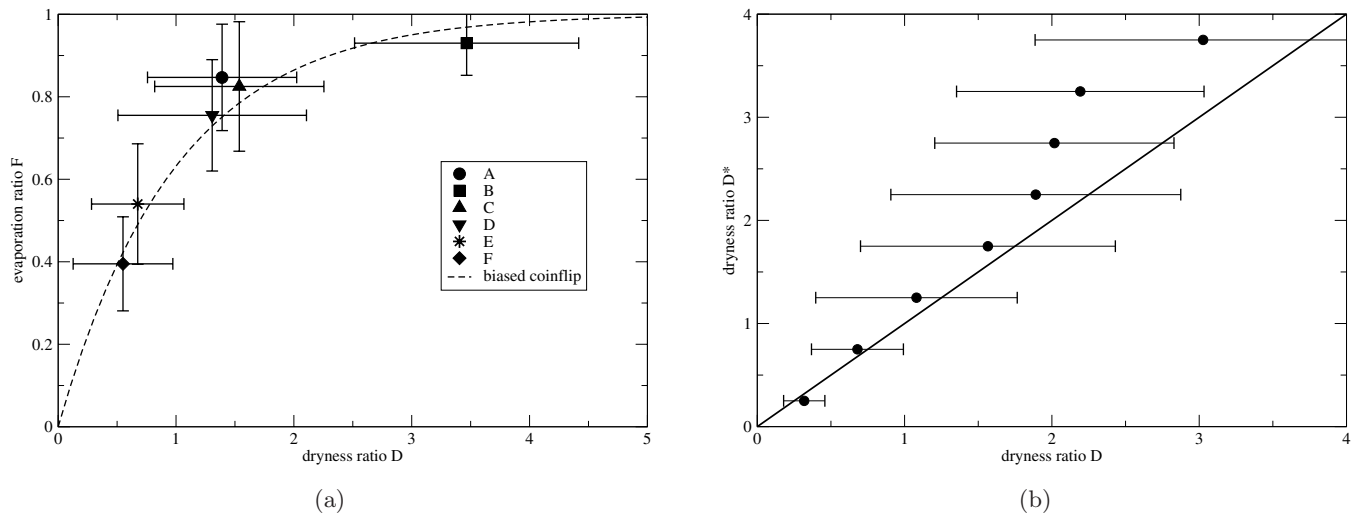


Fig. 3. Validation of the mean flux ratios for vegetation: (a) The dryness D dependent evaporation ratio F^* of the biased coinflip Ansatz (dashed) is compared with Koeppen climate types simulated (ECHAM5 20C) and sampled with respect to dryness and evaporation ratios (large dots and horizontal lines are sample means and standard deviations). (b) The dryness ratio of the biased coinflip Ansatz, $D^* = -\ln(C)$, is compared with the simulated dryness ratio, $D = N/P$.

- (2) *Predictability*: The coupled GCM control run provides a verification set for dryness, $D = N/P$, given by the simulated time averaged net radiation N and precipitation P at all grid-points. The stochastic model prediction (7) of the dryness ratio,

$$D^* = \ln(C)$$

is based on different input from the coupled GCM, namely from the runoff ratio, $C = Ro/P$. Comparison with the GCM dryness ratio, $D = N/P$, is presented in the prediction–verification (D^*, D)-diagram [Fig. 3(b)]: (i) GCM verification D and stochastic model predictions D^* show general agreement with an overall (D^*, D)-correlation of 0.75, which is larger for dryness ratios up to semi-desert regimes, $D^* = 2$. Note the general tendency of a D^* overprediction. (ii) In the energy limited regime ($D < 1$), the D^* -binned standard deviations double per increasing 0.5-dryness ratio units D^* , but remain almost constant beyond. *Summarizing*, the stochastic rainfall–runoff chain’s consistency with the phenomenological (Köppen) climate classes and its predictability (within a consistent data set) encourages us to explore a more physically guided holistic description of land surface climates; that is, extending the analysis of vegetation ($D = N/P$) to rivers ($C = Ro/P = 1 - F$) and to lakes (Sec. 5).

4. Climate Variability and Rivers: Runoff–Rainfall Ratio

A climate state is not only characterized by the mean (as analyzed in the preceding Sec. 4) but also by the variability, which can also be quantified in terms of ratios. Here the focus lies on runoff–rainfall ratios. The climate mean runoff ratio (introduced in Sec. 2), $C = Ro/P$, is analyzed for the biased coinflip approach

$$C^* = 1 - F^* = \exp(-D) \quad (10)$$

and extended to the runoff–rainfall ratios of sensitivity and variance.

- (1) The runoff sensitivity, δRo , of the biased coinflip model (following, for example, [Koster & Suarez, 1999] or [Arora, 2002]) depends on changes of mean precipitation and net radiation, δP and δN , and, after combination with

the water balance, on the dryness ratio D :

$$\delta Ro = \delta P(C - DC_D) + C_D \delta N \quad (11)$$

where the D -derivative of the mean runoff ratio is $C_D = -C$. Squaring, averaging and rearrangement yield the squared runoff sensitivity ratio, which is conveniently interpreted as an approximation of the runoff variance (or standard deviation) ratio:

$$\frac{\langle \delta Ro^2 \rangle}{\langle \delta P^2 \rangle} = \frac{(C - DC_D)^2 + C_D^2 \langle \delta N^2 \rangle}{\langle \delta P^2 \rangle} + \frac{2(C - DC_D)C_D \text{cov}(N, P)}{\langle \delta P^2 \rangle}. \quad (12)$$

Neglecting the net radiation variability, δN , and its rainfall covariance, $\text{cov}(N, P)$, leaves only the first term as relevant which, substituting in the rainfall–runoff chain, yields the link to the mean state runoff–rainfall ratio $C = \exp(-D)$:

$$\frac{\langle \delta Ro^2 \rangle}{\langle \delta P^2 \rangle} \sim (1 + D)^2 C^2. \quad (13)$$

Tests in GCM environments and observations appear to support this ratio of sensitivity [Koster & Suarez, 1999; Arora, 2002].

- (2) The runoff variance ratio can be quantified using the stochastic-dynamic biased coinflip Ansatz. This provides mean and variance of the exponentially distributed rainfall, P and $\sigma_p^2 = P^2$. Water input from the fast biosphere to the soil reservoir, is the day-to-day discharge, $ro_k = p_k - N$, which occurs only if rainfall exceeds the net radiation (or water demand) threshold, $p_k > N$. Thus the climate mean runoff Ro is, as shown in Sec. 2, $Ro = \int_N^\infty (p_k - N) \exp(-p_k/P) dp_k/P = P \exp(-D)$. Its variance, $\sigma_{ro}^2 = \langle ro^2 \rangle - Ro^2$, is

$$\begin{aligned} \sigma_{ro}^2 &= \int_N^\infty \frac{(p_k - N) \exp\left(\frac{-p_k}{P}\right) dp_k}{P} - Ro^2 \\ &= P^2(2 - \exp(-D)) \exp(-D). \end{aligned} \quad (14)$$

The two ratios of runoff–rainfall mean, $C^* = \exp(-D)$, and variance, σ_{ro}^2/σ_p^2 , depend only on the mean water demand and supply, that is, the dryness ratio, D :

$$\frac{\sigma_{ro}^2}{\sigma_p^2} = (2 - C)C. \quad (15)$$

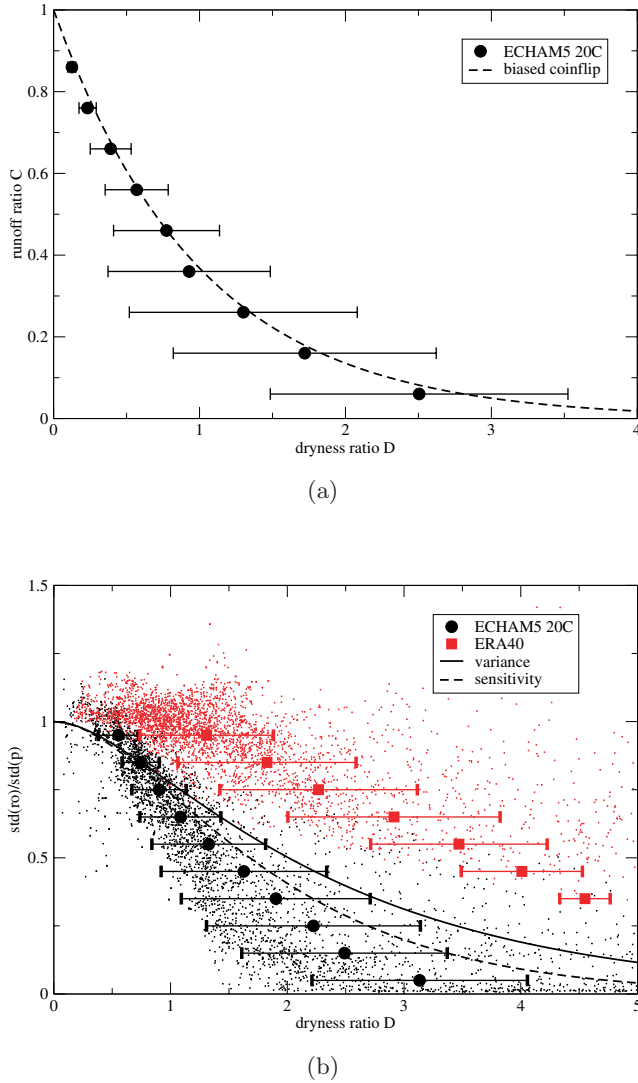


Fig. 4. Validation of the rainfall–runoff flux average and variability ratios: (a) The dryness D dependent runoff ratio C^* of the biased coinflip Ansatz (dashed) is compared with the simulated (ECHAM5 20C) ratio C sampled in bins with means and standard deviations (large dots and horizontal lines). (b) The dryness D dependent runoff–rainfall ratios of sensitivity (dashed) and standard deviation (full) of the biased coinflip Ansatz are compared with the simulated standard deviation ratios (small dots for ECHAM5 20C in black and ERA40 in red) sampled over rainfall–runoff ratio bins (large dots for averages and horizontal lines for standard deviations).

Note that the sum of $k = 1, \dots, K$ independent and exponentially distributed events provides the biased coinflip rainfall totals $p_K = \sum p_k$. They are gamma distributed with mean KP and variance $\sigma_p^2 = KP^2$ corresponding to shape and scale parameter, K and $1/P$. Thus the runoff–rainfall variance ratio also holds for the climate macrostates.

Validation: The runoff–rainfall ratios of means, sensitivities and variances are presented in ratio diagrams (vertical axis) depending on dryness ratio D . The biased coinflip climate [Eq. (10)] is compared with the coupled GCM simulation. The GCM simulated mean runoff ratio (sampled in C -bins) is almost identical with the D -dependent biased coinflip solutions $C^*(D)$. The runoff sensitivity and variance ratios [Fig. 4(b), plotted as standard deviations] determined from annual means of the GCM simulation underestimate the D -dependent solution of the biased coinflip model, whereas the ERA-40 data (analyzed in the same manner) provide a systematic overestimate. This suggests that the biased coinflip climate appears to be most suitable for hydrologically relevant average and variability [Figs. 4(a) and 4(b)] estimates.

5. A New Climate Indicator: Lake Area Ratio

The climatological relevance of the dryness index and its threshold, $D = 1$, separating water and energy limited climates, is demonstrated by another regional surface climate indicator: the lake area ratio. It characterizes terminal lakes, is associated with the long-term water and energy flux balance, and of relevance for paleo-climatic studies. The areas of a closed lake, a_{lake} , and its watershed, a_{land} , define the lake-area ratio:

$$A = \frac{a_{\text{lake}}}{a_{\text{lake}} + a_{\text{land}}}. \quad (16)$$

For ideal topological conditions, lake overflow occurs at $A = 1$ when $a_{\text{land}} = 0$. A parsimonious model of terminal lakes can be derived from the lake area averaged water and energy flux balances; see for example [Kutzbach, 1980] and [Mason *et al.*, 1994]:

$$Ro_{\text{lake}} = P_{\text{lake}} - PE \quad (17)$$

$$N_{\text{lake}} = PE + H_{\text{lake}}. \quad (18)$$

Subscripts denote lake related properties, like runoff (lake inflow), net radiation, and sensible heat fluxes, Ro , N , H , respectively; the lake evaporation is PE . Combining Eqs. (1) and (2) weighted by land and lake areas, a_{lake} and a_{land} , respectively

$$A = \frac{P - E}{PE - E} = \frac{1 - F}{D - F} \quad (19)$$

show that the two climate state components, D and F , enter the lake area ratio. Here the following

closures have been employed to the water and energy flux balances: (i) Precipitation over lake and catchment are assumed to be equal, $P = P_{\text{lake}}$. (ii) Catchment runoff provides the water inflow to the lake, $Ro_{\text{land}} = -Ro_{\text{lake}} a_{\text{lake}}$. (iii) In the long term mean, land and lake are assumed to receive the same energy supply, $N = N_{\text{lake}}$, with lake evaporation balanced by net radiation, $N = N_{\text{lake}} = PE$, equal to the land's potential evaporation.

Closed lakes, $0 < A \leq 1$, occur only under water limited conditions, $\infty < D \leq 1$. The maximum possible lake area ratio, $A = 1$ at $D = 1$, is limited by an idealized catchment size which, when attained, leads to overflow. This lake area ratio reaches its

maximum at $A = 1$, which leads to a (third) threshold correctly separating water from energy limited regimes or closed from open lakes with runoff. Thus it is suggestive to introduce the lake area ratio, A , as an additional component of the surface climate. Employing the biased coinflip world, the terminal lake area ratio A depends only on the dryness ratio D (substituting (8) via (7) to (19))

$$A^* = \frac{\exp(-D)}{D - 1 + \exp(-D)}. \tag{20}$$

In the following the lake area ratios (19) and (20) are analyzed.

5.1. Application

The dryness ratio D of the coupled GCM simulation [Fig. 2(a)] serves as input for the global map of the lake area ratio A [Eq. (19), Fig. 5(a)]; the global distribution of the lake area ratio A (19) is also presented [Fig. 5(b)]. The latter does not invoke the stochastic rainfall-runoff chain as it requires both dryness and evaporation ratio as input fields from the coupled GCM. Both maps are similar. Minor differences occur in regions of South America, South Africa and parts of Central Asia, which may not only be due to insufficiencies of the stochastic rainfall-runoff chain. Overall, application of the stochastic rainfall-runoff chain (7) is suggestive, because it reduces the number of dependent parameters (D and F for A) to the dryness ratio D -dependence only for A^* . This is analyzed

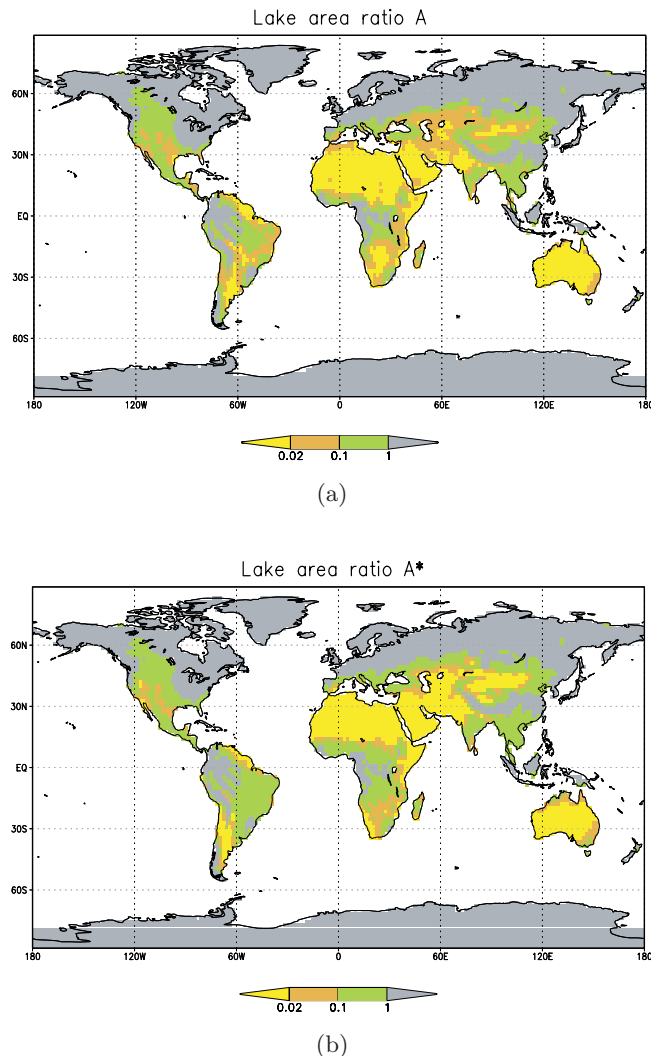


Fig. 5. Present day surface climate maps based on a state of the art coupled atmosphere-ocean GCM (ECHAM5): (a) terminal lake area ratio A based on the simulated mean flux ratios (Eq. (19), D and F); (b) terminal lake area ratio A^* based on the biased coinflip Ansatz (Eq. (20) with D only).

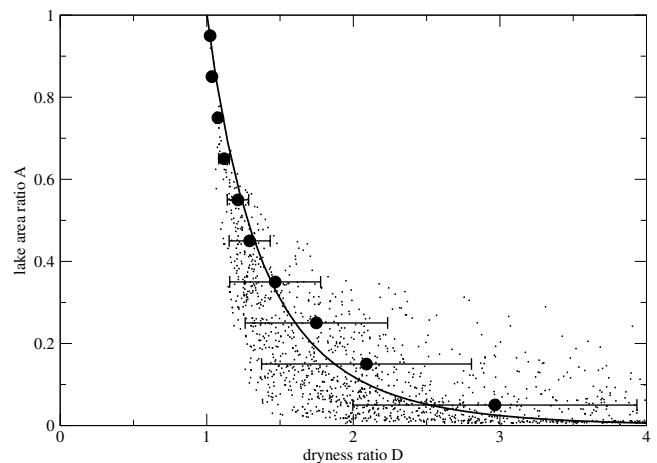


Fig. 6. Validation of the lake area ratio: Dryness D dependent lake area ratio A^* of the biased coinflip Ansatz (dashed) is compared with the simulated lake area ratio A (small dots for ECHAM5 20C in black) sampled over area ratio bins (large dots for averages and horizontal lines for standard deviations).

when employing the subsequent validation procedures. Figure 5 shows the coupled GCM's lake area climate based on (19) and (20) highlighting the threshold $(A, A^*) = 1$, which occurs at the bifurcation $D = 1$ between water and energy limited regimes (green/grey shading). Note that regions with $(A, A^*) = 1$ include all topologically possible terminal lakes, because the threshold is defined by climate conditions (and not by topographic constraints). These are the subtropical areas of central Asia, the North and parts of South Africa, large parts of Australia, and western North America. Note that only water limited regions, $A = 1$, but not the energy limited regions are resolved.

Based on these data the rainfall–runoff chain linked to the lake area diagnostics is validated in

(A, D) -diagram (Fig. 6). (i) The dryness dependent analytical lake area ratio A^* (20) reaches a physically plausible upper bound $A = 1$ at the threshold $D = 1$. That is, this threshold alone demonstrates the validity of the model assumptions underlying the lake area ratio A^* diagnostics and that they are physically and climatologically reasonable. That is, overflow from the terminal lake — with idealized topography, as assumed here — can occur only under energy limited conditions $D = 1$. (ii) The lake area ratio A ((19), dots) deduced from simulated dryness and evaporation ratios, D and F , shows surprisingly good agreement with the dryness D -dependent analytical solution A^* (20) supporting the validity of the rainfall–runoff model (7). (iii) The A -binned D -averages and

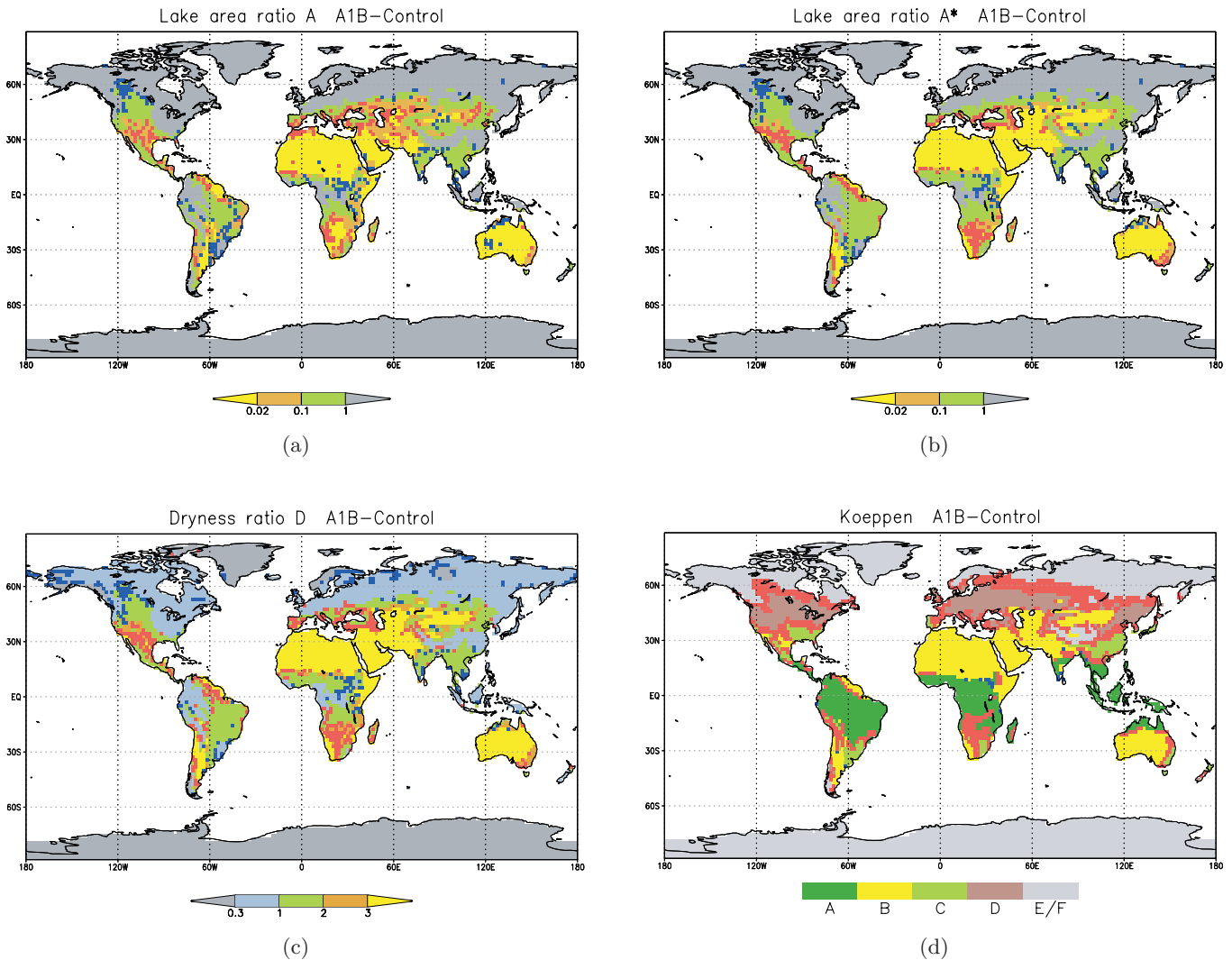


Fig. 7. Climate change analysis: A1B-scenario minus control (ECHAM5 20C, see Fig. 5) of the surface climate: The terminal lake area ratio (A, A^*) is based on (a) two mean flux ratios, D and F (19), and (b) the biased coinflip Ansatz using D (20) only. The climate maps based on (c) Budyko's dryness index D and (d) Koeppen's climate types are also shown. Details of changes are described in the text.

standard deviations of the GCM simulation are well aligned along the D -dependent A^* -graphs of the analytical lake area ratio biased coinflip model. Note that the related standard deviations increase with growing dryness ratio.

Summarizing: The validation shows that the lake area ratio is limited by a physically plausible upper bound at the dryness threshold $D = 1$ from where it decreases continuously with growing dryness. Both threshold and lake area ratio depend on the dryness as the only fundamental climate constant, suggesting it as another viable component of the surface climate state to be presented as a global climate map. In this sense the physics based climate indicators are extended from vegetation (dryness ratio), rivers (runoff ratio) to lakes (lake area ratio). The characteristic climate threshold separating water from energy limited regimes at $D = 1$, emerges also as a feature of the continental landscape, namely as an upper bound for the existence of terminal lakes. In the following section, the new climate map is subjected to IPCC-type climate change analyses.

5.2. Climate change analysis

The present day climate (see Fig. 2 for dryness ratio and Koeppen climate classes, and Fig. 5 for lake area ratios) is compared with the double CO₂ equilibrium surface climate of the A1B scenario [Roeckner *et al.*, 2006] based on a present day state of the art climate model simulation. The results are presented in Fig. 7. (i) Lake area ratio changes are relevant near the threshold $A = 1$ corresponding to the dryness ratio $D = 1$, where closed lakes may pass the threshold to overflow: In the A1B scenario this occurs at the transition from energy limited $D < 1$ to water limited $D > 1$ regimes in the northern great plains of northwest America and also in central Africa [Figs. 7(a)–7(c), blue grid cells]. Accordingly, the lake area ratio indicates a change from closed to open lakes in the northern great plains of America and central Africa. There is less clustering of gridpoints with change in the central parts of Eurasia. (ii) Expansion of dryness [Figs. 7(a)–7(c), red grid cells] is noted in almost all dry regions ($D > 1$) in the subtropics (near 30° latitude, red grid cells) in North and South America, North and South Africa and Eurasia and in south-east Australia. (iii) The Koeppen climate types show similar results: the subtropical type C loses areas to the neighboring dry climate B. The

exception lies at the boundary separating temperate (D) from boreal and ice (E, F) climates. This can be related to the temperature thresholds guiding the Koeppen climate classification, which is not captured by the energy/water flux ratio dependent Budyko dryness index [Fig. 7(d)].

6. Conclusion

We have characterized the Earth's surface cover by climate state parameters, which quantify vegetation by Budyko's dryness ratio D , rivers by the runoff ratio C , and lakes by the terminal lake area ratio A (Fig. 5) using a single fundamental climate parameter: the dryness ratio of water demand to water supply. The theoretical underpinning is provided by stochastic minimalist regional scale climate model based on a biased coinflip Ansatz for the rainfall–runoff chain at the Earth's surface. The model's validation is performed within a state of the art coupled Global Climate Model (GCM) environment, because it provides a physically consistent dataset. Validation analyses show that the consistency and predictability of the stochastic model's climate means and variances are well represented. This suggests that the biased coinflip Ansatz is a viable surrogate for a region's rainfall–runoff affected climate and that it explains the physical aspects of the Earth's near surface climate in a holistic manner comprising vegetation, rivers and lakes as the main natural features. The ideas presented by Fraedrich [2010] on Schreiber's [1904] equation are applied to global data sets. Commencing with the vegetation water capacity and interception being bounded by water demand, a set of further natural thresholds of the land surface climate emerge: the separation between water and energy limited regimes and between closed and overflow lakes.

Future applications are possible: The Schreiber–Budyko relation derived by the surrogate model has provided a powerful diagnostics of the catchment scale surface climate [Sharif *et al.*, 2007; Wang & Takahashi, 1998; Zhang *et al.*, 2004]. The biased coinflip approach may guide climate sensitivity analysis, for example, for applications for paleo-climatic and future climate change scenarios. Given the stochastic background of the biased coinflip rainfall–runoff chain, higher moments may also be determined, for example, drought and wetness based on the standardized precipitation index. Finally, it should be mentioned that the biased coinflip induced relation of the surface climate state

variables bears, in a more general sense, some similarity with the equation of state for ideal gases, where the dryness ratio plays the role of a gas constant.

Acknowledgments

Discussions are appreciated at the Royal Meteorological Institute (Brussels, Febr. 11–12, 2010) workshop on *The Complexity Paradigm: Understanding the Dynamics of Weather and Climate* and at the Isaac Newton Institute (Cambridge 2010) on *Uncertainty in Climate Prediction: Models, Methods and Decision Support*. The Max-Planck-Society is acknowledged for a fellowship. Referees helped to improve the manuscript.

References

- Arora, V. [2002] “The use of the aridity index to assess climate change effect on annual runoff,” *J. Hydrol.* **265**, 164–177.
- Budyko, M. I. [1974] *Climate and Life* (Academic Press), pp. 508.
- Eagleson, P. S. [1978] “Climate, soil, and vegetation, 1. Introduction to water balance dynamics,” *Water Resour. Res.* **14**, 705–712.
- Fraedrich, K., Gerstengarbe, F. W. & Werner, P. C. [2001] “Climate shifts in the last century,” *Clim. Change* **50**, 405–417.
- Fraedrich, K. [2010] “A stochastic parsimonious water reservoir: Schreiber’s 1904 equation,” *J. Hydromet.* **11**, 575–578.
- Guetter, P. J. & Kutzbach, J. E. [1990] “A modified Koeppen classification applied to model simulations of glacial and interglacial climates,” *Clim. Change* **16**, 193–215.
- Hagemann, S., Arpe, K. & Roeckner, E. [2006] “Evaluation of the hydrological cycle in the ECHAM5 model,” *J. Clim.* **19**, 3810–3827.
- Hanasaki, N., Kanae, S., Oke, T., Masuda, K., Motoya, K., Shirakawa, N., Shen, Y. & Tanaka, K. [2008] “An integrated model for the assessment of global water resources — Part 1: Model description and input meteorological forcing,” *Hydrol. Earth Syst. Sci.* **12**, 1007–1025.
- Köppen, W. [1936] *Das Geographische System der Klimate: Handbuch der Klimatologie*, Vol. 1, Part C, Gebr. Bornträger Verl., Berlin, p. 388.
- Koster, R. D. & Suarez, M. J. [1999] “A simple framework examining the interannual variability of land surface moisture fluxes,” *J. Clim.* **12**, 1911–1917.
- Kutzbach, J. E. [1980] “Estimates of past climate at paleolake Chad, North Africa, based on a hydrological and energy balance model,” *Quat. Res.* **14**, 210–223.
- Mason, I. M., Guzkowska, M. A. J., Rapley, C. G. & Street-Perrott, F. A. [1994] “The response of lake levels and areas to climate change,” *Clim. Change* **27**, 161–197.
- Nijssen, B., O’Donnell, G. M., Hamlet, A. F. & Lettenmaier, D. P. [2001] “Hydrologic sensitivity of global rivers to climate change,” *Clim. Change* **50**, 143–175.
- Rodriguez-Iturbe, I., Porporato, A., Ridolfi, L., Isham, V. & Cox, D. R. [1999] “Probabilistic modelling of water balance at a point: The role of climate, soil and vegetation,” *Proc. R. Soc. Lond. A* **455**, 3789–3805.
- Roeckner, E., Lautenschlager, M. & Schneider, H. [2006] “IPCC-AR4 MPI-ECHAM5-T63L31 MPI-OM-GR1.5L40 SRESA1B run no. 1: Atmosphere monthly mean values MPImet/MaD Germany,” *World Data Center for Climate* [doi:10.1594/WDCC/EH5-T63L31-OM-GR1.5L40-A1B-1-MM].
- Savenije, H. H. G. [2004] “The importance of interception and why we should delete the term evapotranspiration from our vocabulary,” *Hydrol. Processes* **18**, 1507–1511.
- Schreiber, P. [1904] “Über die Beziehungen zwischen dem Niederschlag und der Wasserführung der Flüsse in Mitteleuropa,” *Meteorolog. Z.* **21**, 441–452.
- Sharif, H. O., Crow, W., Miller, N. L. & Wood, E. F. [2007] “Multidecadal high-resolution modelling of the Arkansas-Red River basin,” *J. Hydromet.* **8**, 1111–1127.
- Shen, Y. & Chen, Y. [2010] “Global perspective on hydrology, water balance, and water resources management in arid basins,” *Hydrol. Process.* **24**, 129–135.
- Vernadsky, V. I. [1926] *The Biosphere* (Springer-Verlag), pp. 192 ([1998] Translation).
- Wang, Q. & Takahashi, H. [1998] “A land surface water deficit model for an arid and semiarid region: Impact of desertification on the water deficit status in the Loess Plateau, China,” *J. Clim.* **12**, 244–257.
- Zhang, L., Hickel, K., Dawes, W. R., Chiew, F. H. S., Western, A. W. & Briggs, P. R. [2004] “A rational function approach for estimating mean annual evapotranspiration,” *Water Resour. Res.* **40**, W02502 [doi:10.1029/2003WR002710].
- Ziegler, A. D., Sheffield, J., Maurer, E. P., Nijssen, B., Wood, E. F. & Lettenmaier, D. P. [2003] “Detection of intensity in global- and continental-scale hydrological cycles: Temporal scale of evaluation,” *J. Clim.* **16**, 535–547.